frontiers | Frontiers in Environmental Science

TYPE Original Research
PUBLISHED 13 September 2023
DOI 10.3389/fenvs.2023.1254205

OPEN ACCESS

EDITED BY
Lingjun Kong,
Guangzhou University, China

REVIEWED BY
Ivana Smičiklas,
University of Belgrade, Serbia
Koorosh Gharehbaghi,
RMIT University, Australia

*CORRESPONDENCE
C. De Matteis,
chiara.dematteis@unipr.it

RECEIVED 06 July 2023
ACCEPTED 24 August 2023
PUBLISHED 13 September 2023

CITATION
De Matteis C, Mantovani L, Tribaudino M, Bernasconi A, Destefanis E, Caviglia C, Toller S, Dinelli E and Funari V (2023), Sequential extraction procedure of municipal solid waste incineration (MSWI) bottom ash targeting grain size and the amorphous fraction.
Front. Environ. Sci. 11:1254205.
doi: 10.3389/fenvs.2023.1254205

Sequential extraction procedure of municipal solid waste incineration (MSWI) bottom ash targeting grain size and the amorphous fraction

C. De Matteis[1]*, L. Mantovani[1], M. Tribaudino[2], A. Bernasconi[2], E. Destefanis[2], C. Caviglia[2], S. Toller[3], E. Dinelli[4] and V. Funari[3,4,5]

[1]Dipartimento di Scienze Chimiche, della Vita e della Sostenibilità Ambientale, Università di Parma, Parma, Italy, [2]Dipartimento di Scienze della Terra, Università di Torino, Torino, Italy, [3]Consiglio Nazionale delle Ricerche, Istituto di Scienze Marine, CNR-ISMAR Bologna Research Area, Bologna, Italy, [4]Dipartimento di Scienze Biologiche, Geologiche ed Ambientali, Università di Bologna, Bologna, Italy, [5]Dipartimento di Biotecnologie Marine Ecosostenibili, Stazione Zoologica Anton Dohrn, Napoli, Italy

Introduction: Bottom ash (BA) constitutes a significant by-product obtained during the incineration of municipal solid waste in waste-to-energy (WtE) plants. BA is a heterogeneous material made of different fractions, glass, minerals, metals, and unburned residual organic matter. Due to the non-hazardous nature of the unburned material, BA can be effectively recycled, becoming a valuable resource. However, BA displays a high content of potentially toxic elements (PTEs) within its finer grain size. The presence of these elements raises concerns regarding the potential toxicity associated with BA.

Materials and methods: The release of PTEs in the smaller fraction (0.063–0.2 mm; 0.3–0.5 mm; 2–4 mm; bulk <4 mm) of BA collected from the Parma WtE plant was investigated using a new five-step sequential extraction procedure (SEP). Through this method, both leached solutions and solid residues were analyzed by inductively coupled plasma-mass spectroscopy (ICP-MS), X-ray powder diffraction (XRPD), and X-ray fluorescence (XRF) analysis. This integrated approach provided valuable insights into the mineralogy, chemical composition, and PTEs leachability of BA.

Results and discussion: The novelty of this work is the development of a new SEP protocol specifically designed and planned for an anthropogenic material such as BA. The weight reduction recorded after each step is linked to the progressive disappearance of both crystalline and amorphous phases. Water-soluble phases, such as salts, are the first to react, followed by the carbonate fraction in the second step. At the end of the procedure, only quartz, corundum, and Ti-oxide are identified. Among the PTEs, Pb exhibits the highest release, particularly during the acid attack, followed by Zn. The significant release of Ni during the oxidizing and reducing steps can potentially be linked to hydroxides and metallic alloys, respectively. The integration of XRF and Rietveld refinement results on solid residues enabled the identification of several types of amorphous materials and their chemical evolution during the sequential extraction.

KEYWORDS

MSWI-BA, PTEs, SEP, XRPD, XRF, amorphous material, characterization

1 Introduction

"Sustainable cities and communities" and "responsible growth and production" are among the main goals in the United Nations agenda to foster sustainable development worldwide. Among the numerous pillars supporting these goals, waste management plays a crucial role in achieving waste reduction, recycling, and reuse (Kaza et al., 2018; Funari et al., 2023). Incineration of municipal solid waste (MSW) represents an effective approach to waste volume reduction and substantial energy production (Chen et al., 2022). A significant drawback lies in the generation of ashes during the incineration. These ashes are categorized into two main types: bottom ash (BA), which accumulates at the bottom of the burning chamber, and fly ash (FA), formed in the fumes during combustion and subsequently collected by the air-pollution-control systems of the municipal solid waste incineration (MSWI) plant. The recycling of ashes from incineration poses a challenge due to the presence of potentially toxic elements (PTEs) such as Pb, Zn, Cu, Ni, Cd, Cr, and Co (Zhu et al., 2020; Xiang et al., 2022). When MSW is incinerated, the remaining inorganic materials, including PTEs, become concentrated in the ashes. PTEs are elements that can be harmful to human health and the environment at certain concentrations (Domingo et al., 2020; Shi et al., 2020). Currently, only BA is routinely recycled in construction materials, as FA contains higher concentrations and releases PTEs beyond regulatory limits (Blasenbauer et al., 2020).

Due to the mineralogical and chemical heterogeneity of BA, a wealth of mineralogical phases can contain PTEs. These PTEs may occur as impurities in crystalline and glassy phases, and/or they may even constitute the main component of a single phase (Meima and Comans, 1999; Crannell et al., 2000; Dijkstra et al., 2006; Dung et al., 2017; Alam et al., 2019; Loginova et al., 2019; Rissler et al., 2020; De Matteis, 2023). Some of these phases can be soluble, and in order to evaluate the actual release of PTEs, leaching tests were performed according to the UNI EN 12457-2(2004) standard. However, the link between host minerals and leached elements is poorly defined due to the heterogeneity and complex nature of the mineralogical assemblage of the BA. To address this, a sequential extraction procedure (SEP) is employed, as it selectively targets specific fractions during each step of the extraction process. A SEP is an operationally defined methodology that involves a series of selective extractions (Hall et al., 1996). The extractions are done sequentially, with each extraction using a solution of different strength and reactivity. The mineralogical and chemical composition of the residual fraction and of the leachate can be analyzed to determine the host mineral phases and the released elements. This approach allows a better understanding of the association between minerals and leachates for the MSWI BA, and the information obtained can be used to assess the potential environmental risk.

SEPs were originally developed in the 1980s to investigate the chemical composition of the sediments (Tessier et al., 1979; Rapln et al., 1986; Martin et al., 1987). Later, in 1999, a standardized extraction procedure known as the BCR 3-step method (the Community Bureau of Reference, now the European Union "Measurement and Testing Programme") was established (Rauret et al., 1999). However, the application of SEP in BA was relatively limited. The first study was conducted by Sawell et al. (1988), who performed sequential digestion on BA and FA to extract Cd, Pb, Cu, and Zn, aiming to determine their relative solubility. In recent years, there has been a growing interest, and several authors have adapted the BCR 3-step method to waste materials, including BA (Bruder-Hubscher et al., 2002; Haberl and Schuster, 2019), waste from electrical and electronic equipment (Pérez-Martínez et al., 2019), and biomedical waste (Ramesh Kumar et al., 2021). For instance, some authors changed the BCR procedure by adding a fourth step specifically for the residues, without changing the first three (Bruder-Hubscher et al., 2002; Alam et al., 2019). Other authors have taken a step further and developed specific extraction procedures to investigate new materials and waste (Smeda and Zyrnicki, 2002; Abramov et al., 2018; Haberl and Schuster, 2019; Akinyemi et al., 2020). In some cases, a more comprehensive analysis was proposed, where authors determined also the mineralogical composition of the crystalline phases after each step (Abramov et al., 2018; Alam et al., 2019).

Recently, Alam et al. (2019) suggested a new method to examine not only the chemical composition of eluates but also the mineralogical composition of the BA residues, including the quantitative evaluation of the amorphous phases that make up between 30% and 80% of the ashes (Mantovani et al., 2023). The Alam et al. (2019) investigation showed that the standard BCR procedure of dissolving the carbonate fraction with a 0.11 M acetic acid extraction was not able to provide complete carbonate dissolution. Still, no attempt was made to obtain complete dissolution of carbonates using a more acidic extraction.

The aforementioned observation suggests that the standard in BCR, which was calibrated for soils, is not fully applicable in the highly basified environment of BA. This observation aligns with the findings of a recent article by Tong et al. (2020), who examined the FA from MSWI and found that an incomplete acid attack would lead to an underestimation of the leachable PTEs.

In this work, we performed a SEP on BA of different grain sizes using a more acidic environment, aiming at complete dissolution of carbonates. This can be effective for a complex matrix such as the BA, characterized by high carbonate content. Also, we investigated the mineralogical and chemical composition of the solid fractions after each step to better describe the effects of the leaching solutions and directly check the solid phases involved. The mineralogy, including crystalline and amorphous contents, was assessed after each step together with the chemical composition of the residuals and of the leachates.

The SEP was done on BA of small and medium grain sizes (<4 mm), fractions that are more reactive and host a higher concentration of PTEs (Mantovani et al., 2023).

2 Materials and methods

2.1 Description of the samples

BA was sampled at the Parma waste-to-energy plant in June 2021 and had previously undergone detailed characterization in an

TABLE 1 Overview of the five-step sequential extraction procedure used in this work and relative changes or modifications of the standard BCR procedure.

Step	Standard BCR procedure	Step modified in this work	Formula	Dissolved fraction	Information
1	Not present in the standard procedure	Step added in this work: ultrapure water (pH = 7)	H_2O	Exchangeable, water-soluble	Leachable component
2	Acetic acid (0.11 M)	Step changed in this work: acetic acid (5 M)	CH_3COOH	Acid-soluble	Soluble species, cation exchange sites, and carbonates
3	Hydroxylammonium chloride (0.5 M)	Step not changed: hydroxylammonium chloride (0.5 M)	NH_2OH HCl	Reducible	Elements bound to Fe/Mn oxyhydroxides
4	Hydrogen peroxide (8.8 M), ammonium acetate (1 M)	Step not changed: hydrogen peroxide (8.8 M), ammonium acetate (1 M)	H_2O_2, $CH_3CO_2NH_4$	Oxidizable	Elements bound to organic matter and sulfides
5	Not present in the standard procedure	Step added following Huber et al. Perchloric acid, hydrofluoric acid, hydrochloric acid	$HClO_4$, HF, HCl	Residues	Silicate-based materials and well-crystallized oxides

earlier study (Mantovani et al., 2021; De Matteis, 2023). The waste input (tons/year) is represented by undifferentiated MSW of 126.317 t/y and special waste (construction and demolition waste, sewage sludge, cemetery waste, biomedical waste, etc.) of 33.515 t/y that generated 32.904 t/y of BA (Iren Ambiente, 2022). The plant employs grate furnace technology, where the waste is incinerated for 2–3 h at temperatures ranging from 750°C to 1,000°C. The sampling was carried out during the process activity in different time intervals; the samples were randomly collected from a stockpile that was 2–3 m high, which is representative of more than 1 month of accumulation. About 13 kg of BA was collected from the plant. Before the analysis, the ashes were mixed, dried in an oven at 50°C for 24 h, and sieved to separate them into distinct size classes. The sequential sieving process (Φ: 16, 8, 4, 2, 1, 0.5, 0.3, 0.2, and 0.063 mm) was performed according to the European standards for aggregates EN 933–2 (Ente Nazionale Italiano di Unificazione, 2020).

The SEP was done on four selected particle sizes (0.063–0.2 mm; 0.3–0.5 mm; 2–4 mm; and <4 mm) that were split with Quantachrome macro and micro rifflers to obtain 1 g samples. The selected grain sizes represent fine, medium, and bulk fractions of the BA-MSWI. Of these, 20 g was randomly selected and processed for each grain size. At the end of each extraction step, three samples were taken. The solid residues were dried in an oven at 60°C, weighed, and analyzed with X-ray powder diffraction (XRPD) and X-ray fluorescence (XRF) analysis, while the eluates were analyzed using inductively coupled plasma-mass spectroscopy (ICP-MS). The BA used was relatively fresh, being analyzed just a few weeks after the sampling.

2.2 Sequential extraction procedure

2.2.1 Reagents

For all experiments, ultrapure water (UPW) (Milli-Q® 18.2 MΩ.cm at 25°C and TOC < 5 ppb) obtained from a water purification system (Merck Millipore) was used. The following reagents were also used: acetic acid glacial (100% for analysis, VWR); hydroylammonium chloride (pure, VWR); hydrogen peroxide (30% stabilized, VWR); ammonium acetate (pure for analysis, Merck); hydrofluoric acid (48% ultrapure, Sigma-Aldrich), perchloric acid (70% for analysis, Acros Organics); nitric acid (65% for analysis, Merck); and hydrochloric acid (37% for analysis, Honeywell Fluka).

2.2.2 5 - Steps sequential extraction procedure

Starting from the standard and modified BCR procedure (Smeda and Zyrnicki, 2002; Abramov et al., 2018; Haberl and Schuster, 2019; Akinyemi et al., 2020), a new five-step SEP was set in this work (Table 1). The SEP has been specifically adapted for BA, incorporating additional steps and modifications compared to the BCR standard method. The primary changes implemented are as follows.

The standard BCR procedure does not include a specific step for water-soluble phases similar to the leaching test procedure UNI EN 12457-2. However, in materials like BA, the presence of these phases is significant. The recycling of BA is linked to the results of leaching tests, where the release of PTEs from partially or completely water-soluble phases such as ettringite, hydrocalumite, and salts is evaluated. Notably, these phases become more significant in aged BA, resulting in increased leachability (Mantovani et al., 2023). By including a dedicated step for water-soluble phases in the extraction procedure, we allow for a more comprehensive investigation of their leaching behavior.

Previous studies have indicated that the BCR standard acid attack was not efficient for BA (Alam et al., 2019; Haberl and Schuster, 2019). In this study, XRPD analysis of the residue treated with 0.11 M acetic acid revealed that the carbonate phases only dissolved after 18 washing cycles. Consequently, a higher molarity of acetic acid or a different acid solution was needed for effective carbonate removal. After multiple attempts, a more concentrated acetic acid solution (5 M) was used, with the pH buffered at pH = 2.8, resulting in the complete dissolution of carbonates.

At the end of the procedure, the remaining phases ideally consist of an amorphous fraction, silicates, and well-crystallized oxides, which are expected to be abundant in BA (Mantovani et al., 2023). In agreement with previous literature (Bruder-Hubscher et al., 2002; Alam et al., 2019; Haberl and Schuster, 2019; Pérez-Martínez et al., 2019), a final dedicated step for the complete removal of the more resistant phases has been included in our modified SEP.

Step 1. (**Water-soluble fraction**): In centrifuge tubes (50 mL), 1 g of BA and 40 mL of UPW were added. The samples were shaken in an orbital shaker at 30 rpm for 16 h (overnight) at room temperature. Then, the solid fraction was separated from the liquid by centrifugation at 3,000 rpm for 20 min (or until all

suspended particles were precipitated). The eluates filtered using a filter apparatus (0.45 μm) with a vacuum pump. This step was added to the three-step BCR after consulting literature data (Flyhammar, 1998; Smeda and Zyrnicki, 2002; Abramov et al., 2018; Haberl and Schuster, 2019) to better investigate the behavior of soluble phases in BA.

Step 2. (**Carbonate fraction**): In centrifuge tubes (50 mL), 40 mL of 5 M acetic acid (CH_3COOH) was added to each solid residue from the prior step. The samples were shaken in an orbital shaker at 30 rpm for 16 h (overnight) at room temperature. Then, the solid fraction was separated from the liquid by centrifugation at 3,000 rpm for 20 min. The eluates were filtered using a filter apparatus (0.45 μm) with a vacuum pump. Solid residues were washed with UPW three times in a centrifuge. This step was changed with respect to the BCR and other experiments found in the literature after several unsuccessful carbonate removal tests.

Step 3. (**Reducible fraction**): Residues from the previous extraction were added to 40 mL hydroxylammonium chloride ($NH_2OH * HCl$) 0.5 M. The samples were shaken in an orbital shaker at 30 rpm for 16 h (overnight) at room temperature. The solid fraction was separated from the liquid by centrifugation at 3,000 rpm for 20 min. The eluates were recovered using a filter apparatus (0.45 μm) with a vacuum pump. The solid residues are washed with UPW three times in a centrifuge. This step is the same as the one in the BCR described by Rauret et al. (1999).

Step 4. (**Oxidizable fraction**): The solid residues from the third step were placed in glass beakers with 10 mL of hydrogen peroxide (H_2O_2). The beakers were covered with a watch glass, and the sample was digested at room temperature for 1 h with occasional manual shaking. The digestion continued for 1 h at 85°C in a thermostatic bath, and then the volume was reduced to less than 3 mL by further heating of the uncovered beakers. After that, an aliquot of 10 mL of hydrogen peroxide was added, the beakers were covered, and the digestion continued at 85°C for another hour. The watch glasses were removed, and the volume of the liquid was reduced to about 1 mL. The solid residues were transferred to a centrifuge tube, and 50 mL of ammonium acetate ($CH_3CO_2NH_4$) 1.0 M was added. The samples were shaken in an orbital shaker at 30 rpm for 16 h (overnight) at room temperature. Then, the solid fraction was separated from the liquid by centrifugation at 3,000 rpm for 20 min. The eluates were obtained through a vacuum pump filter apparatus (0.45 μm). The solid residues were washed with UPW three times in a centrifuge. This step is the same as the step in the standard BCR (Rauret et al., 1999).

Step 5. (**Residuals**): The last step is designed to remove silicates and well-crystallized oxides. Solid residues from Step 4 were transferred to Teflon beakers and digested with a 5:1 mixture of hydrofluoric and perchloric acids. First, a solution of concentrated $HClO_4$ (2 mL) and HF (10 mL) was added, which reacted completely. Then, another aliquot of $HClO_4$ (1 mL) and HF (10 mL) was added. Finally, $HClO_4$ (1 mL) was poured into the becker, and the residue was dissolved with HCl 12 N and diluted to 25 mL. Any remaining solid was transferred to a centrifuge tube and washed three times with UPW by centrifugation at 3,000 rpm for 20 min. This step followed the procedure described in Bruder-Hubscher et al. (2002). ICP analysis was not done at this stage.

After each step, three solid residues were characterized by XRPD and XRF; their respective eluates were filtered, collected, and stored with three drops of HNO_3 at a temperature of 4°C. Blank solutions were prepared at each step.

2.3 X-ray powder diffraction (XRPD) and Rietveld analysis

For each sieved part, XRPD was performed at the end of each step of the extraction procedure. A Bruker D2 Phaser powder diffractometer with θ-θ focalizing geometry was used, operating at 30 kV and 10 mA with Cu Kα (λ = 1.54178 Å) radiation. Data were measured in the 5°–100° 2θ range, with a 0.02° step size and a 1 s/step counting time. Each sample was spun at 30 rpm.

EVA identification software (Bruker) and Crystallography Open Database (COD) were used to indentify the major crystalline phases. Only phases with a concentration higher than 1% can routinely be identified. This generally rules out the detection of phases where PTEs are present as main constituents, e.g., smithsonite and cerussite.

The RIR-Rietveld method was applied by spiking with 10 wt.% high-purity silicon to quantify the major crystalline phases and the amorphous fraction (Gualtieri, 2000). The Rietveld refinements were performed using the GSAS and EXPGUI packages (Toby and Von Dreele, 2013; Larson and Von Dreele, 2004). Scale factors, cell parameters, and pseudo-Voigt profile coefficients for each phase were refined, as well as the instrumental zero. The background was also refined manually, using a 10-term Chebychev polynomial. The ICSD reference numbers for each crystalline phase involved in the Rietveld refinement are summarized in Supplementary Table S1.

The qualitative analysis results are summarized in Supplementary Table S2, and the quantitative results obtained using the RIR-Rietveld method are listed in Supplementary Table S3. The quantitative results are expressed as the RIR-Rietveld results normalized to 100% (including the estimated amorphous fraction) times the residual weight fraction to correct for the weight loss.

2.4 X-ray fluorescence (XRF) analysis

The chemical composition of each sieved portion was measured at the end of each step using a wavelength dispersive X-ray fluorescence (XRF) spectrometer, Panalytical Axios 4000, equipped with an Rh tube. About 3 g of the representative samples were oven-dried at 50°C, homogenized, and milled with an agate vibratory disk mill. Pressed powder pellets for XRF analysis were prepared using a boric acid binder. The reproducibility, general accuracy through the calibration curve, and corrections of the data were the same as those used in other works (Franzini et al., 1972; Toller et al., 2021). Major (SiO_2, TiO_2, Al_2O_3, Fe_2O_3, MnO, MgO, CaO, Na_2O, K_2O, and P_2O_5), minor, and trace element (As, Ba, Br, Ce, Cl, Co, Cr, Cu, Ga, Hf, La, Mo, Nb, Ni, Pb, Rb, S, Sc, Sn, Sr, Th, U, V, W, Y, Zn, and Zr) concentrations were calculated using a calibration curve built on a large number of certified reference

10.3389/fenvs.2023.1254205

TABLE 2 X-ray fluorescence (XRF) spectrometry analysis of major (a) and minor and trace elements **(b)** for different grain sizes and different steps (from S0 to S4).

a)		Major element (g/100 g)										
Grain size (mm)	Step	SiO_2	TiO_2	Al_2O_3	Fe_2O_3	MnO	MgO	CaO	Na_2O	K_2O	P_2O_5	LOI
0.063–0.2	S0	19.38	0.98	11.60	2.71	0.10	2.96	32.93	2.38	1.30	1.91	23.76
	S1	19.16	0.89	12.27	2.50	0.09	2.93	30.17	1.05	0.79	1.79	18.91
	S2	12.11	1.18	7.87	2.49	0.05	0.81	3.12	0.52	0.48	1.26	6.07
	S3	11.98	1.18	7.81	2.45	0.04	0.78	2.57	0.49	0.43	1.05	5.71
	S4	11.48	1.10	7.01	2.37	0.03	0.68	1.26	0.44	0.42	0.52	3.26
0.3–0.5	S0	31.36	0.97	14.20	4.07	0.11	3.30	25.15	3.57	1.65	1.75	14.00
	S1	30.46	0.95	14.58	3.86	0.11	3.16	24.73	2.07	1.33	1.73	12.44
	S2	23.80	1.28	10.83	3.76	0.07	1.37	4.30	1.41	1.00	1.29	4.17
	S3	24.76	1.17	10.57	3.95	0.06	1.33	3.28	1.36	0.94	1.15	4.15
	S4	24.27	1.04	9.14	3.74	0.05	1.23	2.19	1.31	0.86	0.71	2.88
2–4	S0	48.01	0.69	10.83	4.89	0.14	3.35	16.97	5.32	1.76	1.09	6.99
	S1	50.70	0.75	11.25	4.36	0.12	3.35	14.90	4.81	1.52	0.79	4.64
	S2	42.54	0.90	7.79	3.80	0.08	3.02	7.85	4.00	1.35	0.73	2.49
	S3	39.28	0.80	9.54	3.60	0.07	2.84	5.04	3.23	1.20	0.69	2.06
	S4	32.76	0.67	5.92	3.48	0.04	1.49	3.89	2.36	0.90	0.62	0.94
<4	S0	34.57	1.09	13.29	4.71	0.11	3.51	26.72	3.13	1.73	1.83	10.30
	S1	33.09	0.95	14.53	3.90	0.09	3.43	23.28	3.07	1.30	1.53	9.61
	S2	34.34	0.89	9.33	3.70	0.07	2.31	5.94	2.81	0.99	0.89	2.46
	S3	35.04	0.73	9.61	3.60	0.05	2.22	4.82	2.31	0.97	0.78	1.46
	S4	31.41	1.01	9.34	3.02	0.04	1.82	4.66	2.03	0.89	0.72	1.42
b)		Minor element (mg/kg)										
Grain size (mm)	Step	Mo	Pb	Sr	Br	Ba	Co	Cr	Cu	Ni	S	V	Zn
0.063–0.2	S0	18	850	501	54	411	4	569	870	122	39,030	42	6,830
	S1	13	926	422	9	496	5	465	817	146	31,099	37	6,676
	S2	10	287	122	3	510	17	588	338	142	1,235	54	1,368
	S3	10	258	63	4	474	19	606	241	113	1,224	49	1,285
	S4	6	134	37	1	643	12	422	210	83	1,940	38	1,050
0.3–0.5	S0	9	720	292	26	690	10	552	1,250	153	21,750	37	6,560
	S1	9	508	281	7	605	12	530	662	141	19,065	51	6,876
	S2	9	205	86	2	650	21	769	646	161	1,910	56	1,627
	S3	4	203	41	n.d.	690	20	635	641	194	1,061	53	1,413
	S4	4	90	35	n.d.	469	25	666	403	90	308	48	1,303
2–4	S0	19	430	294	13	573	10	907	390	173	8,350	42	4,760
	S1	19	465	135	n.d.	548	13	560	593	173	2,869	39	2,091
	S2	15	69	129	n.d.	552	9	610	316	195	2,113	40	1,006
	S3	15	63	65	n.d.	620	23	879	230	134	621	44	1,039
	S4	n.d.	16	46	n.d.	422	20	775	75	65	364	37	846

(Continued on following page)

TABLE 2 (*Continued*) X-ray fluorescence (XRF) spectrometry analysis of major (a) and minor and trace elements **(b)** for different grain sizes and different steps (from S0 to S4).

a)		Major element (g/100 g)											
Grain size (mm)	Step	SiO_2	TiO_2	Al_2O_3	Fe_2O_3	MnO	MgO		CaO	Na_2O	K_2O	P_2O_5	LOI
<4	S0	13	410	434	26	720	10	489	830	177	23,200	42	5,360
	S1	13	106	286	4	650	20	531	751	103	17,904	36	4,476
	S2	11	136	162	3	732	17	491	905	152	1,248	42	3,461
	S3	11	113	114	2	410	14	534	440	130	703	36	1,149
	S4	11	90	101	n.d.	480	24	376	336	90	324	30	1,408

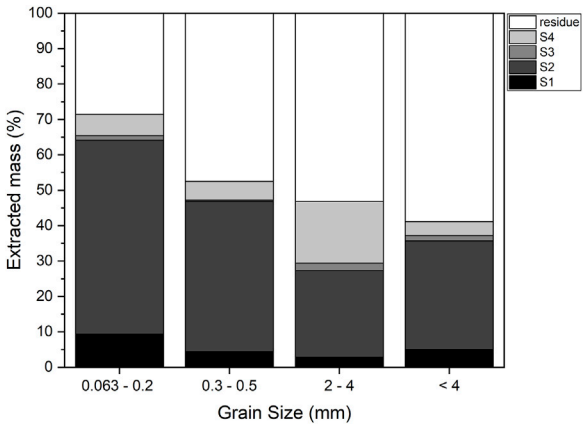

FIGURE 1
Extracted mass (%) for different steps of the extraction procedure and different grain sizes.

materials and offline correction of loss on ignition (LOI) values. LOI, which is correlated with the influence of humidity, organic matter, and water, was gravimetrically estimated after overnight heating of the samples at 950°C in a muffle furnace (Heiri et al., 2001). The XRF results for different grain sizes and different steps are reported in Table 2. These results are expressed as the analytical value times the residual weight fraction to correct for the weight loss.

2.5 Inductively coupled plasma mass spectroscopy (ICP-MS)

Sample solutions were filtered with a 0.45-μ filter and acidified with super pure nitric acid. Several elements (Fe, Mn, Ti, Li, V, Cr, Ni, Cu, Zn, Mo, Cd, and Pb) were analyzed using an Agilent 7500 ICP-MS system. The standard solution used for the calibration setting was a Carlo Erba 504310 Multielement Standard of 100 mg/L in 5% HNO_3.

The leached amount of a given element at each step was obtained from the results considering the weight loss and the dilution of the sample with the formula:

$$El_{leached} = \frac{(El_{measured} \cdot dil)}{wt}, \quad (1)$$

where $El_{leached}$ is the fraction of each element (in mg/kg) leached from the sample after each step, $El_{measured}$ is the measured concentration (in mg/mL), *wt* is the weight loss calculated from the ratio of the measured weight after each step (mg) and that of the starting sample, and *dil* is the volume (L) in which the sample is diluted.

3 Results

3.1 Weight loss, XRPD, XRF, and ICP-MS results

First step. The weight loss after each step is shown in Figure 1 and Supplementary Table S4. From a mineralogical point of view, this loss is linked to the progressive disappearance of crystalline phases and amorphous material, depending on their reactivity with different reagents (Figure 2).

After the first step, there was a mild but significant weight loss, ranging from 3% in the larger grain size to 9% in the smaller one. As reported in Mantovani et al. (2023), the higher weight loss in major elements occurred for Ca, Na, and K, together with S and Cl. These elements were found in the leachate as they are present in highly soluble phases such as chlorides, anhydrite, and hydrocalumite. XRPD showed that chlorides and anhydrite disappeared, and hydrocalumite decreased significantly (Supplementary Tables S2, S3 and Figure 3).

The slight decrease in Ca (Table 2 and Supplementary Figure S1) is explained through XRPD results by the total dissolution of portlandite ($Ca(OH)_2$), partial dissolution of larnite (Ca_2SiO_4), and the decrease in amorphous cement phases (Supplementary Tables S2, S3 and Figure 3). An increase in the amorphous material was found in larger grain-size fractions (2–4 mm), likely due to the reprecipitation of dissolved crystalline phases (Alam et al., 2019). The smaller grain size also showed a partial dissolution of the amorphous material. The decreased amorphous material accounted for the higher weight loss in the smaller grain-size fractions.

Second step. We observed a considerable weight loss in the second step of between 27% and 54% in the larger and smaller grain sizes, respectively. The loss was clear for Al, Ca, and Mg in any grain size, and Si in smaller ones. Also, LOI showed a high reduction in value (from about 30% in the 2–4 mm grain size to 69% in <4 mm grain size), probably represented by the loss of

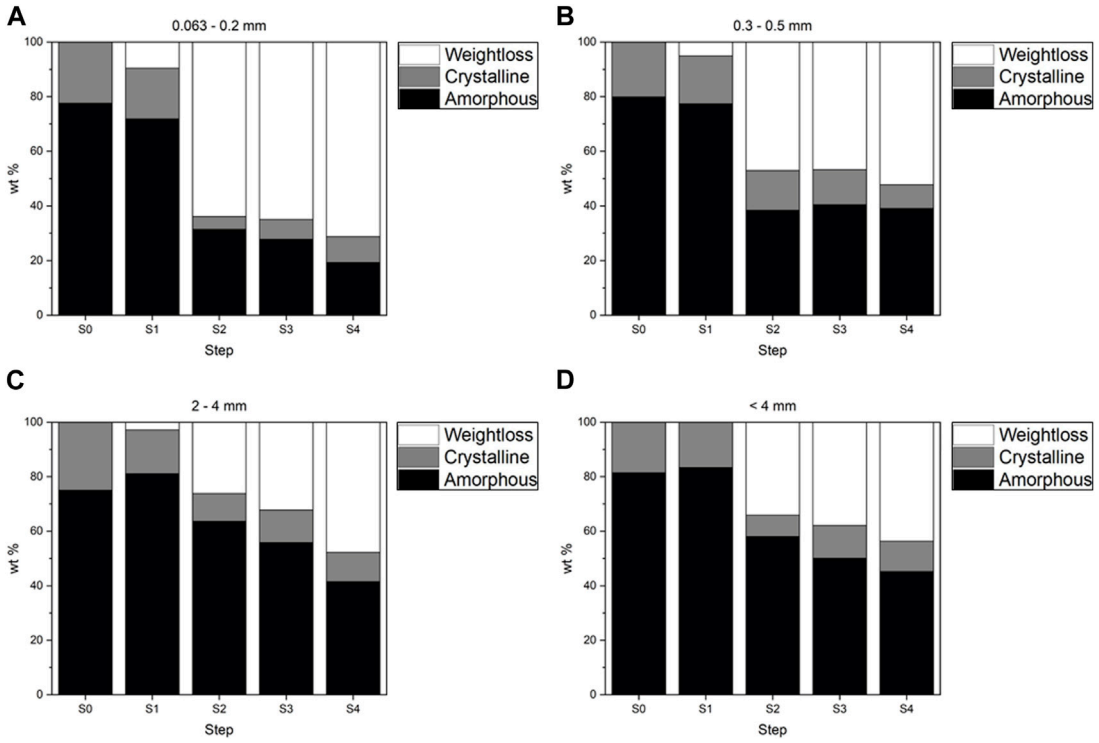

FIGURE 2
Quantitative Rietveld analysis (wt%) of the crystalline and amorphous components after the different steps (from S0 to S4) for each grain size [**(A)** 0.063–0.2 mm, **(B)** 0.3–0.5 mm, **(C)** 2–4 mm, **(D)** <4 mm).

CO_2 (Table 2 and Supplementary Figure S1). Ca decreased more in smaller grains: in the analysis of the residuals, we saw that 80% of the total Ca in the 0.063–0.2 mm grain size was leached at this stage, while only 40% was leached in the 2–4 mm grain size. The disappearance of Ca-rich phases as calcite, larnite, and hydrocalumite and the removal and the decrease of melilite in smaller and larger grains can partially explain the large decrease in Ca. However, all the aforementioned crystalline phases together did not account for more than 25% (on average) of the total Ca weight loss. The observed weight loss was primarily due to a strong dissolution of the amorphous fraction (Supplementary Table S3 and Figure 2).

Sulfur showed a strong decrease: in the 2–4 mm grain size, about 25% of the S present in the starting material solubilizes, and about 90% of the S solubilizes in the smaller grain size (Table 2). Despite this decrease, no sulfate crystalline phase dissolved at this stage, with the exception of minor hydrocalumite. It appeared that S was present within a poorly or non-diffracting phase, either nanocrystalline or amorphous. μ-XRF and XANES analysis showed an alteration rim S enriched in some grains (De Matteis, 2023), which is likely to be washed during the first two steps. The S in the rims was related to highly soluble sulfates, suggesting their formation during weathering.

Overall, we found a higher dissolution than reported by Alam et al. (2019) in this second step. In Alam et al. (2019), the acid reaction reduced the smaller fraction (≤0.125 mm) and the larger one (0.125–1 mm) to 35% and 20% of the original value, while in our work, the reduction was higher, being between 64% (0.063–0.2 mm) and 27% (2–4 mm). The higher dissolution in the second step is an effect of the higher concentration of acetic acid. The basic environment of the BA buffers the pH of the solution, and the acid attack is less effective. If we accept that the purpose of the second step is to completely dissolve the carbonates, the standard BCR is not suitable for a material like BA. At the end of the second step, Fe and Al oxides (hematite and magnetite, corundum) were identified in the XRPD pattern, while they were not visible in the starting pattern due to the overlapping peaks (Supplementary Tables S2, S3).

Third step. The third step led to a barely detectable weight reduction, confirmed by slight changes in the diffraction pattern. The same behavior was observed in the work of Alam et al. (2019), probably due to the smaller quantity of reducible phases in the BA.

Fourth step. A significant weight reduction occurred after the fourth step, up to 20% of the original weight in the 2–4 mm size fraction and between 5% and 7% in the other fractions (Figure 1).

We hypothesized that the reduction of LOI value (about 2% in all grain sizes) is probably due to the loss of organic matter.

Moreover, the removal of the sulfides, due to their oxidation to sulfates and subsequent dissolution, is a likely explanation for the decrease of S in the residual fraction in all grain sizes, especially in the smaller ones (Table 2).

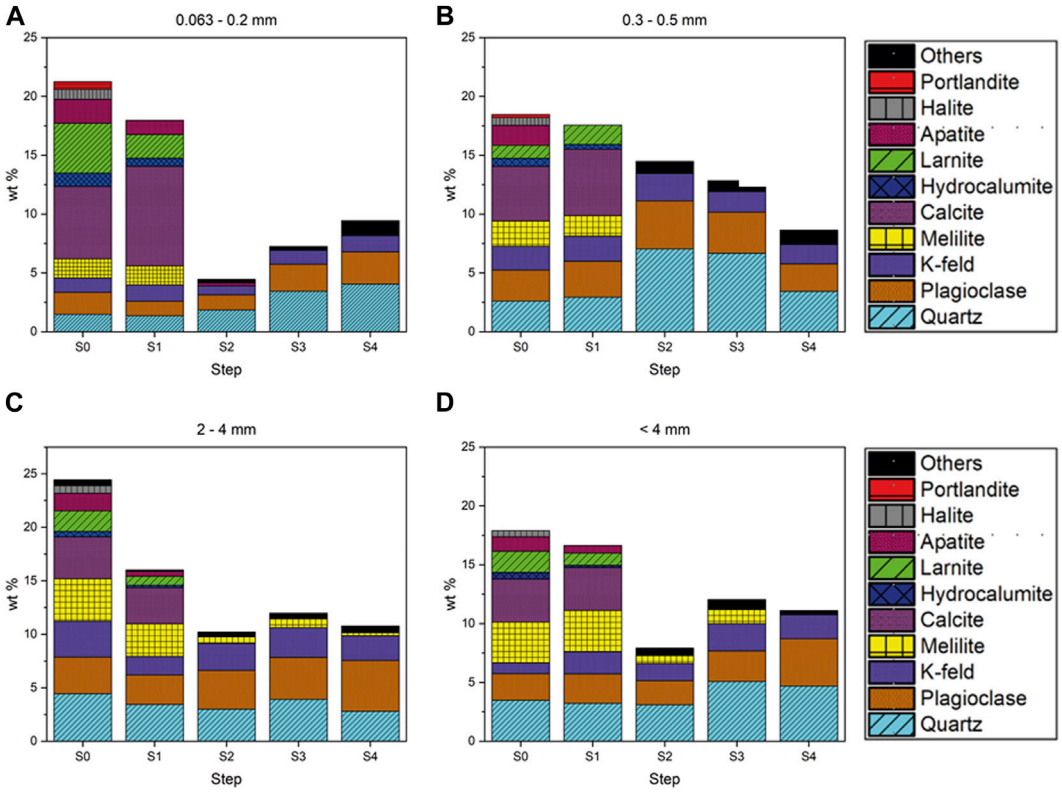

FIGURE 3
Quantitative Rietveld analysis (wt%) of the crystalline component after each step (from S0 to S4) for each grain size [**(A)** 0.063–0.2 mm, **(B)** 0.3–0.5 mm, **(C)** 2–4 mm, **(D)** <4 mm].

The residual crystalline phases, feldspars, and quartz were quite stable until the end of the fourth step. After the sequential extraction, some elements, such as S and Ca, were almost completely leached, indicating that they are not concentrated in silicate crystals, glass, or resistant oxides, like spinels.

After the third and fourth steps, the weight loss was very similar in the different size portions (Figure 1 and Supplementary Table S4), in accord with Alam et al. (2019).

Fifth step. After the hydrofluoric (HF) and perchloric ($HClO_4$) acid attack, the amorphous and crystalline phases were almost completely dissolved. The non-soluble fraction weighed less than 3% of the original fraction, down to 1% for the smaller grains (Supplementary Table S4). Due to the scarcity of the residual material, chemical characterization was not done, while XRPD analysis showed only quartz, corundum, and a Ti-oxide (Supplementary Figure S2).

3.2 Sequential extraction of critical raw elements

The leaching of a few elements (Pb, Cu, Zn, Mn, Ni, Fe, Cr, Ti, and Ba) was investigated by ICP-MS analysis after each step (Table 3). The elements showed different behaviors, likely tied to different mineralogical and/or amorphous environments. Due to the heterogeneity of BA, it is difficult to create a link between the element and the hosting phase: the element may be present as an impurity or as a major constituent of a given phase. In the latter case, such phases are present at a concentration below 1% and are not detected by XRPD. This could explain the high release of some elements, such as Pb and Zn, even if no mineralogical phase with these elements was identified by XRPD.

First step. In the first step, the almost negligible release of Fe and Cu (Table 3 and Figure 4) suggests that these elements are not present as the primary component in salts or water-soluble phases or in the small portion of amorphous fraction that reacts at this step (Figure 2), although we could not exclude their presence as impurities within these phases.

Second step. In the second step, several elements exhibited a significant level of extraction (Table 3 and Figure 4). Pb, Zn, and Cu were the highly leached elements, showing an extracted amount between 50% and 70% of their original budget (Figure 4).

Almost all of the leached Zn was extracted in this step, recording a release of about 70% in both grain sizes (Figure 4). XANES analysis found Zn to be typically associated with carbonates, such as smithsonite ($ZnCO_3$) or hydrozincite [$Zn_5(CO_3)_2(OH)_6$], or with hydroxides, such as $Zn(OH)_2$, that are leached by acid attack (Rissler et al., 2020; De Matteis, 2023). Moreover, Zn was found in melilite solid solution, that is, hardystonite (Mantovani et al., 2021); this could account for some leached Zn, as melilite showed a major decrease in this step.

TABLE 3 Elemental analysis (mg/kg) of the eluates extracted during the procedure (from S1 to S4) from the grain sizes 0.3–0.5 mm and <4 mm.

Grain size (mm)	0.3–0.5				<4			
Step	S1	S2	S3	S4	S1	S2	S3	S4
Element	mg/kg							
Ti	1	159	13	24	2	196	9	42
Cr	3	40	22	45	4	52	19	34
Mn	2	249	36	5,286	3	277	35	41
Fe	86	7,194	495	465	121	5,841	580	257
Ni	4	25	59	86	4	31	51	70
Cu	23	499	57	819	28	396	76	844
Zn	3	3,158	42	69	15	3,495	48	52
Ba	7	11	52	96	7	9	83	49
Pb	106	288	75	119	7	501	78	106

The leached fraction of Pb ranged between 47% and 64% in larger and smaller grains (Figure 4), respectively. XANES analysis showed that Pb could be present as a carbonate and as Pb_3O_4; both phases are unstable in a highly acidic environment (Brookins, 1978). Also, other oxide phases found in SEM-EDS analysis of the BA (De Matteis, 2023), such as Ca_2PbO_4, are soluble in an acid environment (Jernejcic et al., 1969).

Cu showed a moderate release at this step, about 35% for <4 mm and 22% for the 0.3–0.5 mm grain size (Figure 4). Its presence can be inferred as a carbonate phase, as reported by Rissler et al. (2020), and within the amorphous phases that are removed in this step.

Also, Fe, Mn, and Cr showed a higher release in this step than the others, although not as significant as Zn, Pb, and Cu. This is likely related to their presence in carbonates, oxides, or hydroxides, which dissolve in acidic conditions.

Third step. A significant relative Ni extraction was observed, although the dissolved quantities were limited. In fact, the extraction of Ni in this stage with respect to the total Ni content was about 22% in the <4 mm grain size and 14% in the 0.3–0.5 mm grain size (Figure 4). Also, Pb and Ba showed some association with these fractions, both with a release of about 10%. For Ba, this is the step where higher extraction was observed. At this stage, Fe/Mn oxyhydroxide dissolution was rather small, shown by the small extracted amount of Fe and Mn (Table 3 and Figure 4). It is likely that they were already dissolved in the second step for a strong association with acid-soluble phases. Some dissolution of the amorphous fraction was observed at this stage, which could account for the loss of Ni, Ba, and Pb.

Fourth step. Ni and Cu were the most leached elements in the oxidizing step. For Cu, it was about 50% of the bulk composition. SEM-EDS and XANES analyses showed that both elements were commonly found as metal droplets within a silicate matrix that are oxidized in a soluble ionic species (Mantovani et al., 2021; De Matteis, 2023).

Residues

From Figure 4, it appears that the elements with an overall sum of extracted fractions and mostly related to residual phases are Ti (95% in both fractions), Cr (around 80%), Fe (around 80%), Ba (around 75%), and, to a minor extent, Mn and Ni at least in the 0.3–0.5 mm grain size. Cr, Fe, Mn, and Ti can be present in silicate glasses or in spinel oxides; Ba can likely occur as an impurity in feldspars.

In contrast, Pb, Zn, and Cu were only marginally present in the residual fraction (Figure 4). Microprobe analysis showed that Zn, Cu, and Pb are present in silicate glasses as impurities (Mantovani et al., 2021); moreover, Zn was found in spinel oxides. Also, Zn was observed in silicates like willemite or in solid solution in feldspars. Pb could also be present in feldspars (Benna et al., 1996; Tribaudino et al., 2005).

4 Discussion

4.1 A new SEP for the assessment of BA

The sequential extraction of BA does not have a validated procedure. The use of the standard BCR procedure in the second step of the reaction with acetic acid likely underestimates the release under acidic conditions. Flyhammar (1998) used a concentration of NaAc 1 M at pH 5.0 to anaerobically degrade MSW, showing a decrease of up to 57% in weight after the second step for grains below 2 mm. Alam et al. (2019) used a solution of 0.11M HOAc at pH 2.85, but a complete dissolution of calcite through this step was not reached. With the same conditions, we measured a pH of about 5, and the dissolution of calcite was not observed.

Unlike the outcome reported by Alam et al. (2019), a significant decrease in the plagioclase content was never observed; we found instead a strong decrease in the amorphous fraction. In addition, Alam et al. (2019) found a very limited extraction of Pb, Ni, Cr, and Cu in the acetic acid attack and minimal extraction of Zn.

In this work, the major extraction of Zn with Pb and Cu, and minor quantities of Cr, Fe, and Mn, suggest that these critical raw elements might be in carbonate phases. Abramov et al. (2018)

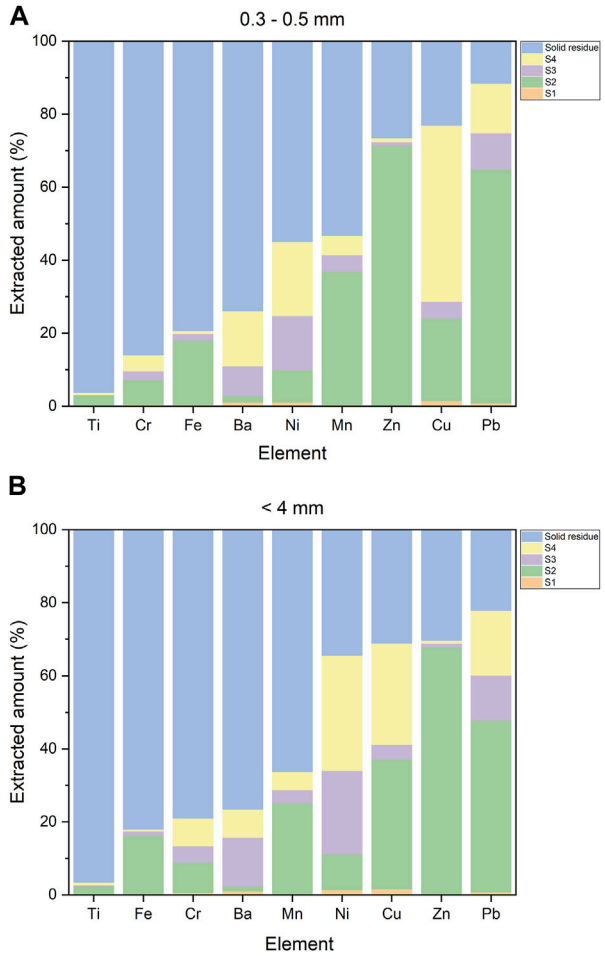

FIGURE 4
Extracted amount (%) of some critical elements by ICP-MS for **(A)** 0.3–0.5 mm grain size and **(B)** <4 mm grain size. The values of the solid residue correspond to the XRF analysis.

studied a mixture of BA and FA, adopting the standard BCR procedure. The mineralogy after each step was not reported, so the amount of the amorphous fraction could not be assessed. However, the pH determined after the acid extraction step was between 4.3 and 5, higher in the case of smaller grain sizes. Again, Abramov et al. (2018) had a lesser extraction of PTEs after the acetic acid attack, with a release of 34% Zn and 9% Pb. Extractions in the oxidizable and reducible fractions were of the same magnitude, consistent with Alam et al. (2019).

Tong et al. (2020) repeated washing with acetic acid to achieve complete carbonate dissolution in FA. After washing, they found that the pH decreased from 12 to 3.8, which is still above the dissolution limits for carbonates. In our case, the attempt to dissolve carbonates using 0.11 M acetic acid occurred only after 18 washes, a figure that significantly extends the procedure's timeline.

Tong et al. (2020) observed a higher release of Mn than Fe in the acetic acid attack, as was also found in this work. After repeated acid washing, they found that the leachable fractions of Zn and Pb were 68% and 54%, respectively, in line with our results. Cu leaching was much higher in our results, up to 94%; a lower but significant release of Ni and Cr was also observed in Tong et al. (2020).

Haberl and Schuster (2019) analyzed both FA and BA from MSWI, using the fraction below 0.3 mm, using a seven-step procedure, where the acetic acid attack is reported in the fourth step. Instead of using acetic acid in a defined concentration, they added pure acetic acid during the extraction to keep the pH at 3, following the work of Van Herck and Vandecasteele (2001). This corresponds to keeping the pH conditions constant for the dissolution of carbonates. After the acetic acid attack, 50% and 65% of the original Pb and Zn, 50% and 30% of Cu and Ni, less than 10% of Cr and Fe, and 30% of Mn were released. The method, however, is not fully comparable to our results because the acid attack in their method happens before the steps dedicated to the removal of water-soluble phases and to an ion exchange process.

The proposed methodology should not be seen as definitive. The use of sequential extraction allows for the investigation of the release of some critical elements from incinerator residues at a deeper level of detail. However, it is necessary to emphasize that these residues exhibit significant heterogeneity over time (seasonal variations) and space (different facilities with diverse technologies and different collected waste). Certainly, it is valuable to observe the release as a function of different environments (i.e., at different pH values), with the purpose of optimizing the recovery of the PTEs and understanding their release in the environment.

4.2 Composition of amorphous phase(s)

The amorphous phase represents a large fraction in all investigated residues (Supplementary Table S3 and Figure 2) that changes in the different steps of the sequential extraction. We examined the compositional heterogeneities in the amorphous phase by combining XRF and RIR-Rietveld analyses of the residues.

For a given *n*th sequential step, the contribution of the *i*th major oxide to the residual amorphous chemical composition ($Ar_{n,i}$) has been determined by means of the following equation:

$$Ar_{n,i} = C_{n,i} - \sum_{k=1,N} W_{n,k} S_{i,k}, \quad (2)$$

where $C_{n,i}$ is the content of the *i*th major oxide measured by XRF analysis for the *n*th sequential step; $W_{n,k}$ is the weight % of the *k*th crystalline phase as from the RIR-Rietveld analysis for the *n*th sequential step (Supplementary Table S3); $S_{i,k}$ is the stoichiometric content of the *i*th major oxide in the *k*th crystalline phase, as from chemical formula in Supplementary Table S1; and *N* is the total number of the involved crystalline phases.

The residual amorphous normalized chemical composition for the *n*th sequential step ($Ar\_norm_{n,i}$) is obtained by normalization to 100%.

The full results are shown in terms of $Ar_{n,i}$ (Supplementary Table S5) and $Ar\_norm_{n,i}$ (Supplementary Table S6). The former leads one to appreciate major oxide variations from step to step, while the latter leads one to appreciate the residual amorphous composition at each step. The results are also plotted in a Ca-Al-Si ternary diagram for each size fraction (Figure 5).

The starting amorphous composition is different from size to size, with higher silica for the larger grains, suggesting an

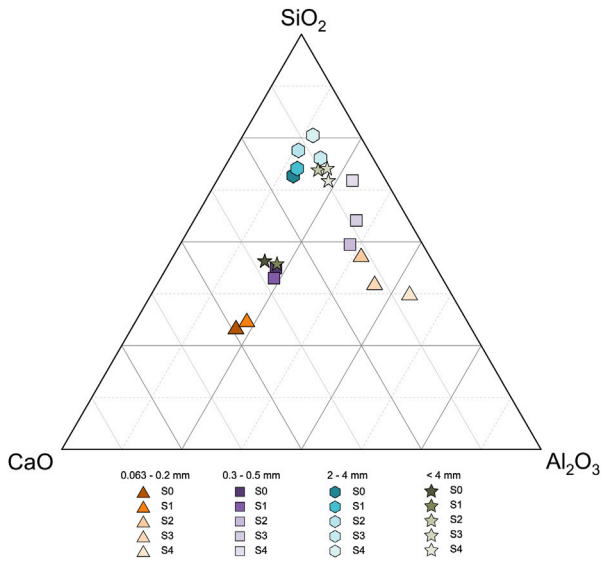

FIGURE 5
Ternary diagram of the amorphous fraction composition for the different grain sizes. Different grain sizes are represented by different colors (orange: 0.063–0.2 mm, violet: 0.3–0.5, blue: 2–4 mm, and gray: <4 mm). The amorphous composition of the starting material is represented by the darker hues of the different colors that gradually become lighter as the steps progress.

enrichment of silica-based glass in this granulometric fraction in accordance with Mantovani et al. (2021). After the first step, the glass composition appears like the starting one, although in the two finer grain sizes (i.e., the sizes with larger weight loss), Na_2O and K_2O are diluted in the residual amorphous phase, suggesting that some amorphous Na/K-bearing soluble gel is present at the initial stage, as found in Mantovani et al. (2023).

After the second step, the Ca content massively decreases. This effect is larger in the finer grain sizes, with an *Ar_norm* decrease of 22% and 15% for the 0.063–0.2 mm and 0.3–0.5 mm fractions, respectively. Al_2O_3 also decreases (3–4 wt.% for all grain sizes), while SiO_2 loses from 6% to 11 wt.% of the original weight, except in the <4-mm fraction.

In light of these values, the second step significantly changes the residual amorphous composition, whose chemical character can be addressed by the decomposition of Ca-Si-Al-rich compounds. In fact, as shown by Inkaew et al. (2016), the amorphous/microcrystalline C-S-H represents an important quench product, also confirmed by the article by Saffarzadeh et al. (2011) that showed a variety of amorphous Ca-Al-Si-rich hydrates.

These complex hydrate phases are similar to the phases of paste cement, which undergo destabilization/corrosion when decreasing the pH of the solution. This phenomenon depends on several parameters like the acid concentration, and it appears along with Ca ion release in the solution (Pavlik, 1994). This mechanism would explain the loss of CaO, or at least part of it, due to its moderate dissolution rate, but not the losses of SiO_2 and Al_2O_3. For the loss of these two species and possibly CaO, we may invoke the dissolution of glass formed during the melting process in the incinerator (Bayuseno and Schmahl, 2010; Mantovani et al., 2021). This melting process leads to a complex Ca-rich aluminosilicate glass, a material whose behavior in an acid environment can approach that of slags with a similar composition, which are known to undergo acetic acid dissolution easily and quickly (Song et al., 2017). Moreover, the presence of some CaO released by amorphous calcium carbonate cannot be excluded, as mentioned by Santos et al. (2013).

The third step is the most conservative, as the weight loss is absent for all four investigated grain sizes. Therefore, we can state that only little reducible amorphous fraction is present.

In contrast, there is evidence of oxidizable fraction loss. Part of it (1%–2.5% wt., depending on the grain size) can be related to organic matter, which is another type of amorphous product generated by the incinerator (Bayuseno and Schmahl, 2010).

In consideration of the different amorphous materials extracted at the different stages, Figure 5 proposes a chemical trend where the residual amorphous composition progressively shifts toward Si-enriched material.

5 Conclusion

In this work, chemical and mineralogical analyses of BA from the Parma MSWI plant were performed on the residue of each step of a sequential extraction. Chemical analysis was also carried out on the corresponding leachate after each step.

The main results are as follows:

1) A revised SEP was tested, with the main purpose of obtaining the full dissolution of carbonates in the acetic acid step. The highly basic environment of BA prevents the complete dissolution of carbonate phases, following standard BCR, as the pH solution remains significantly higher than 3. In order to dissolve the carbonate phases, the molarity of the solution was increased, allowing us to investigate the behavior of PTEs in BA's carbonates in acid environments. This promoted higher leaching of Zn and Pb than was found in previous investigations. Zn and Pb were most leached in the second step, indicating their presence in carbonates and acid-soluble phases.
2) Due to the extreme heterogeneity of the material, it was not possible to rely on standard BCR by increasing the number of acid-washing cycles. Easier or tougher dissolution of carbonates may depend on the nature of the BA and be related to parameters such as aging, feed waste type, and incineration strategy. We propose, therefore, the use of concentrated acetic acid to keep the pH = 3.
3) The amorphous phase represents a very large fraction of the investigated residues. The combination of XRF and RIR-Rietveld analyses at the different sequential steps allowed us to distinguish between different types of amorphous material, possibly Na/K-bearing soluble gels, organic matter, C-S-H products, melt glass, and Si-enriched residues, with the latter three being larger in content. The dissolution of the amorphous phases is much higher in small grain sizes, likely explaining the difference in the weight loss between different grain sizes.
4) Among crystalline phases, the cement-related phases, such as hydrocalumite, larnite, and portlandite, disappear in the first and

second steps, whereas feldspars and quartz do not significantly change during the extraction procedure.

5) The investigated elements were poorly represented in the reducible phase, except for Ni, Ba, and Pb, whereas the association with the oxidizable fraction was significant for Cu and Ni. Lastly, the highest percentages of Ti, Cr, Fe, Ba, and Mn were found in the residual phase.

Data availability statement

The original contributions presented in the study are included in the article/Supplementary Material; further inquiries can be directed to the corresponding author.

Author contributions

CD: Conceptualization, Data curation, Methodology, Writing–original draft, Writing–review and editing. LM: Conceptualization, Data curation, Writing–original draft, Writing–review and editing. MT: Writing–review and editing, Conceptualization, Data curation, Writing–original draft. AB: Data curation, Methodology, Writing–review and editing. EDe: Data curation, Methodology, Writing–review and editing. CC: Data curation, Methodology, Writing–review and editing. ST: Data curation, Methodology, Writing–review and editing. EDi: Data curation, Methodology, Writing–review and editing. VF: Data curation, Methodology, Writing–review and editing.

Funding

This research was financially supported by the program "BANDO ATENEO per la ricerca 2021" of the University of Parma, PRIN 2017 2017L83S77_005 "Mineral reactivity, a key to understand large-scale processes: from rock forming environments to solid waste recovering/lithification and Research Grant in memory of Prof. Fiorenzo Mazzi of the Italian Society of Mineralogy and Petrology (SIMP)." In addition, this work benefited from the equipment and framework of the COMP-HUB and COMP-R Initiatives, funded by the "Departments of Excellence" program of the Italian Ministry for University and Research (MIUR, 2018–2022 and MUR, 2023–2027). This research is part of the project NODES, which has received funding from the MUR–M4C2 1.5 of PNRR with grant agreement no. ECS00000036.

Acknowledgments

The authors thank Enrico Maria Selmo, Andrea Comelli, and Luca Barchi for their constant support during the laboratory activities.

Conflict of interest

The authors declare that the research was conducted in the absence of any commercial or financial relationships that could be construed as a potential conflict of interest.

Publisher's note

All claims expressed in this article are solely those of the authors and do not necessarily represent those of their affiliated organizations, or those of the publisher, the editors, and the reviewers. Any product that may be evaluated in this article, or claim that may be made by its manufacturer, is not guaranteed or endorsed by the publisher.

Supplementary material

The Supplementary Material for this article can be found online at: https://www.frontiersin.org/articles/10.3389/fenvs.2023.1254205/full#supplementary-material

References

Abramov, S., He, J., Wimmer, D., Lemloh, M. L., Muehe, E. M., Gann, B., et al. (2018). Heavy metal mobility and valuable contents of processed municipal solid waste incineration residues from Southwestern Germany. *Waste Manag.* 79, 735–743. doi:10.1016/j.wasman.2018.08.010

Akinyemi, S. A., Gitari, W. M., Thobakgale, R., Petrik, L. F., Nyakuma, B. B., Hower, J. C., et al. (2020). Geochemical fractionation of hazardous elements in fresh and drilled weathered South African coal fly ashes. *Environ. Geochem. Health* 42, 2771–2788. doi:10.1007/s10653-019-00511-3

Alam, Q., Schollbach, K., van Hoek, C., van der Laan, S., de Wolf, T., and Brouwers, H. J. H. (2019). In-depth mineralogical quantification of MSWI bottom ash phases and their association with potentially toxic elements. *Waste Manag.* 87, 1–12. doi:10.1016/j.wasman.2019.01.031

Bayuseno, A. P., and Schmahl, W. W. (2010). Understanding the chemical and mineralogical properties of the inorganic portion of MSWI bottom ash. *Waste Manag.* 30, 1509–1520. doi:10.1016/j.wasman.2010.03.010

Benna, P., Tribaudino, M., and Bruno, E. (1996). The structure of ordered and disordered lead feldspar (PbAl2Si2O8). *Am. Mineral.* 81, 1337–1343. doi:10.2138/am-1996-11-1205

Blasenbauer, D., Huber, F., Lederer, J., Quina, M. J., Blanc-Biscarat, D., Bogush, A., et al. (2020). Legal situation and current practice of waste incineration bottom ash utilisation in Europe. *Waste Manag.* 102, 868–883. doi:10.1016/j.wasman.2019.11.031

Brookins, D. G. (1978). Eh-pH diagrams for elements from Z = 40 to Z = 52: Application to the Oklo natural reactor, Gabon. *Chem. Geol.* 23, 325–342. doi:10.1016/0009-2541(78)90086-4

Bruder-Hubscher, V., Lagarde, F., Leroy, M. J. F., Coughanowr, C., and Enguehard, F. (2002). Application of a sequential extraction procedure to study the release of elements from municipal solid waste incineration bottom ash. *Anal. Chim. Acta* 451, 285–295. doi:10.1016/S0003-2670(01)01403-9

Chen, D., Zhang, Y., Xu, Y., Nie, Q., Yang, Z., Sheng, W., et al. (2022). Municipal solid waste incineration residues recycled for typical construction materials—A review. *RSC Adv.* 12, 6279–6291. doi:10.1039/d1ra08050d

Crannell, B. S., Eighmy, T. T., Krzanowski, J. E., Eusden, J. D., Shaw, E. L., and Francis, C. A. (2000). Heavy metal stabilization in municipal solid waste combustion bottom ash using soluble phosphate. *Waste Manag.* 20, 135–148. doi:10.1016/S0956-053X(99)00312-8

De Matteis, C. (2023). *Mineralogical and chemical characterization of Bottom Ahes from waste incineration*.

Dijkstra, J. J., Van Der Sloot, H. A., and Comans, R. N. J. (2006). The leaching of major and trace elements from MSWI bottom ash as a function of pH and time. *Appl. Geochem.* 21, 335–351. doi:10.1016/j.apgeochem.2005.11.003

Domingo, J. L., Marquès, M., Mari, M., and Schuhmacher, M. (2020). Adverse health effects for populations living near waste incinerators with special attention to hazardous

waste incinerators. A review of the scientific literature. *Environ. Res.* 187, 109631. doi:10.1016/j.envres.2020.109631

Dung, T. T. T., Vassilieva, E., Golreihan, A., Phung, N. K., Swennen, R., and Cappuyns, V. (2017). Potentially toxic elements in bottom ash from hazardous waste incinerators: an integrated approach to assess the potential release in relation to solid-phase characteristics. *J. Mater. Cycles Waste Manag.* 19, 1194–1203. doi:10.1007/s10163-016-0505-0

Ente Nazionale Italiano di Unificazione (2020). Tests to determine the geometric characteristics of aggregates—Part 2: Determination of the particle size distribution—control sieves, nominal dimensions of the openings. *UNI En.* 933-2, 2020.

Flyhammar, P. (1998). Use of sequential extraction on anaerobically degraded municipal solid waste. *Sci. Total Environ.* 212, 203–215. doi:10.1016/S0048-9697(97)00339-2

Franzini, M., Leoni, L., and Saitta, M. (1972). A simple method to evaluate the matrix effects in X-Ray fluorescence analysis. *X-Ray Spectrom.* 1, 151–154. doi:10.1002/xrs.1300010406

Funari, V., Toller, S., Vitale, L., Santos, R. M., and Gomes, H. I. (2023). Urban mining of municipal solid waste incineration (MSWI) residues with emphasis on bioleaching technologies: a critical review. *Environ. Sci. Pollut. Res.* 30, 59128–59150. doi:10.1007/s11356-023-26790-z

Gualtieri, A. (2000). Accuracy of XRPD QPA using the combined Rietveld–RIR method. *J. Appl. Crystallogr.* 33, 267–278. doi:10.1107/S002188989901643X

Haberl, J., and Schuster, M. (2019). Solubility of elements in waste incineration fly ash and bottom ash under various leaching conditions studied by a sequential extraction procedure. *Waste Manag.* 87, 268–278. doi:10.1016/j.wasman.2019.02.001

Hall, G. E. M., Vaive, J. E., Beer, R., and Hoashi, M. (1996). Selective leaches revisited, with emphasis on the amorphous Fe oxyhydroxide phase extraction. *J. Geochem. Exp.* 56 (1), 59–78. doi:10.1016/0375-6742(95)00050-X

Heiri, O., Lotter, A. F., and Lemcke, G. (2001). Loss on ignition as a method for estimating organic and carbonate content in sediments: reproducibility and comparability of results. *J. Paleolimnol.* 25, 101–110. doi:10.1023/A:1008119611481

Inkaew, K., Saffarzadeh, A., and Shimaoka, T. (2016). Modeling the formation of the quench product in municipal solid waste incineration (MSWI) bottom ash. *Waste Manag.* 52, 159–168. doi:10.1016/j.wasman.2016.03.019

Iren Ambiente (2022). *Dichiarazione ambientale 2021 polo ambientale integrato di Parma*.

Jernejcic, J., Skledar, S., and Sencar, J. (1969). Synthesis and characterization of calcium orthoplumbate (Ca_2PbO_4). *Indus Eng. Chem-Product Res. Dev.* 8, 149–154. doi:10.1021/i360030a010

Kaza, S., Yao, L. C., Bhada-Tata, P., and Woerde, F. V. (2018). *What a waste 2.0: A global snapshot of solid waste management to 2050. NW*. Washington, D.C.: The World Bank Pubblication.

Larson, A. C., and Von Dreele, R. B. (2004). *General structure analysis system (GSAS)(Report LAUR 86-748).* Los Alamos, NM: Los Alamos National Laboratory.

Loginova, E., Volkov, D. S., van de Wouw, P. M. F., Florea, M. V. A., and Brouwers, H. J. H. (2019). Detailed characterization of particle size fractions of municipal solid waste incineration bottom ash. *J. Clean. Prod.* 207, 866–874. doi:10.1016/j.jclepro.2018.10.022

Mantovani, L., De Matteis, C., Tribaudino, M., Boschetti, T., Funari, V., Dinelli, E., et al. (2023). Grain size and mineralogical constraints on leaching in the bottom ashes from municipal solid waste incineration: a comparison of five plants in northern Italy. *Front. Environ. Sci.* 11, 1–15. doi:10.3389/fenvs.2023.1179272

Mantovani, L., Tribaudino, M., De Matteis, C., and Funari, V. (2021). Particle size and potential toxic element speciation in municipal solid waste incineration (Mswi) bottom ash. *Sustain* 13, 1–17. doi:10.3390/su13041911

Martin, J. M., Nirel, P., and Thomas, A. J. (1987). Sequential extraction techniques: Promises and problems. *Mar. Chem.* 22, 313–341. doi:10.1016/0304-4203(87)90017-X

Meima, J. A., and Comans, R. N. J. (1999). The leaching of trace elements from municipal solid waste incinerator bottom ash at different stages of weathering. *Appl. Geochem.* 14, 159–171. doi:10.1016/S0883-2927(98)00047-X

Pavlik, V. (1994). Corrosion of hardened cement paste by acetic and nitric acids part I: Calculation of corrosion depth. *Cem. Conc. Res.* 24, 551–562.

Pérez-Martínez, S., Giro-Paloma, J., Maldonado-Alameda, A., Formosa, J., Queralt, I., and Chimenos, J. M. (2019). Characterisation and partition of valuable metals from WEEE in weathered municipal solid waste incineration bottom ash, with a view to recovering. *J. Clean. Prod.* 218, 61–68. doi:10.1016/j.jclepro.2019.01.313

Ramesh Kumar, A., Vaidya, A. N., Singh, I., Ambekar, K., Gurjar, S., Prajapati, A., et al. (2021). Leaching characteristics and hazard evaluation of bottom ash generated from common biomedical waste incinerators. *J. Environ. Sci. Heal. - Part A Toxic/Hazardous Subst. Environ. Eng.* 56, 1069–1079. doi:10.1080/10934529.2021.1962159

Rapln, F., Tessler, A., Campbell, P. G. C., and Carignan, R. (1986). Potential artifacts in the determination of metal partitioning in sediments by a sequential extraction procedure. *Environ. Sci. Technol.* 20, 836–840. doi:10.1021/es00150a014

Rauret, G., López-Sánchez, J. F., Sahuquillo, A., Rubio, R., Davidson, C., Ure, A., et al. (1999). Improvement of the BCR three step sequential extraction procedure prior to the certification of new sediment and soil reference materials. *J. Environ. Monit.* 1, 57–61. doi:10.1039/a807854h

Rissler, J., Klementiev, K., Dahl, J., Steenari, B. M., and Edo, M. (2020). Identification and quantification of chemical forms of Cu and Zn in MSWI ashes using XANES. *Energy Fuels* 34, 14505–14514. doi:10.1021/acs.energyfuels.0c02226

Saffarzadeh, A., Shimaoka, T., Wei, Y., Gardner, K. H., and Musselman, C. N. (2011). Impacts of natural weathering on the transformation/neoformation processes in landfilled MSWI bottom ash: A geoenvironmental perspective. *Waste Manag.* 31, 2440–2454. doi:10.1016/j.wasman.2011.07.017

Santos, R. M., Mertens, G., Salman, M., Cizer, Ö., and Van Gerven, T. (2013). Comparative study of ageing, heat treatment and accelerated carbonation for stabilization of municipal solid waste incineration bottom ash in view of reducing regulated heavy metal/metalloid leaching. *J. Environ. Manage.* 128, 807–821. doi:10.1016/j.jenvman.2013.06.033

Sawell, S. E., Bridle, T. R., and Constable, T. W. (1988). Heavy metal leachability from solid waste incinerator ashes. *Top. Catal.* 6, 227–238. doi:10.1177/0734242x8800600140

Shi, Y., Li, Y., Yuan, X., Fu, J., Ma, Q., and Wang, Q. (2020). Environmental and human health risk evaluation of heavy metals in ceramsites from municipal solid waste incineration fly ash. *Environ. Geochem. Health* 42, 3779–3794. doi:10.1007/s10653-020-00639-7

Smeda, A., and Zyrnicki, W. (2002). Application of sequential extraction and the ICP-AES method for study of the partitioning of metals in fly ashes. *Microchem. J.* 72, 9–16. doi:10.1016/S0026-265X(01)00143-6

Song, K., Park, S., Kim, W., Jeon, C. W., and Ahn, J. W. (2017). Effects of experimental parameters on the extraction of silica and carbonation of blast furnace slag at atmospheric pressure in low-concentration acetic acid. *Met. (Basel)* 7, 199–214. doi:10.3390/met7060199

Tessier, A., Campbell, P. G. C., and Bisson, M. (1979). Sequential extraction procedure for the speciation of particulate trace metals. *Anal. Chem.* 51, 844–851. doi:10.1021/ac50043a017

Toby, B. H., and Von Dreele, R. (2013). GSAS-II: The genesis of a modern open-source all purpose crystallography software package. *J. Appl. Crystallogr.* 46, 544–549. doi:10.1107/S0021889813003531

Toller, S., Funari, V., Vasumini, I., and Dinelli, E. (2021). Geochemical characterization of surface sediments from the Ridracoli reservoir area and surroundings, Italy. Details on bulk composition and grain size. *J. Geochem. Explor.* 231, 106863. doi:10.1016/j.gexplo.2021.106863

Tong, L., He, J., Wang, F., Wang, Y., Wang, L., Tsang, D. C. W., et al. (2020). Evaluation of the BCR sequential extraction scheme for trace metal fractionation of alkaline municipal solid waste incineration fly ash. *Chemosphere* 249, 126115. doi:10.1016/j.chemosphere.2020.126115

Tribaudino, M., Benna, P., Nestola, F., Meneghini, C., and Bruno, E. (2005). Thermodynamic behaviour of the high-temperature $\bar{P}1$-$\bar{I}1$ phase transition along the CaAl2Si2O8 -SrAl2Si208 join. *Phys. Chem. Min.* 32, 314–321. doi:10.1007/s00269-005-0469-4

Van Herck, P., and Vandecasteele, C. (2001). Evaluation of the use of a sequential extraction procedure for the characterization and treatment of metal containing solid waste. *Waste Manag.* 21, 685–694. doi:10.1016/S0956-053X(01)00011-3

Xiang, G., Qiu, J., Li, Z., Chen, J., and Song, Y. (2022). Eco-friendly treatment for MSWI bottom ash applied to supplementary cementing: Mechanical properties and heavy metal leaching concentration evaluation. *Constr. Build. Mater.* 327, 127012. doi:10.1016/j.conbuildmat.2022.127012

Zhu, Y., Zhao, Y., Zhao, C., and Gupta, R. (2020). Physicochemical characterization and heavy metals leaching potential of municipal solid waste incinerated bottom ash (MSWI-BA) when utilized in road construction. *Environ. Sci. Pollut. Res.* 27, 14184–14197. doi:10.1007/s11356-020-08007-9